RSC Advances

PAPER

View Article Online
View Journal | View Issue

Open Access Article. Published on 11 November 2022. Downloaded on 1/12/2026 3:45:44 PM.
This article is licensed under a Creative Commons Attribution-NonCommercial 3.0 Unported Licence.

Check for updates

Cite this: *RSC Adv.*, 2022, **12**, 32219

An antibacterial chitosan-based hydrogel as a potential degradable bio-scaffold for alveolar ridge preservation

Xiaoyu Zhou,†[a] Congrui Liu,†[c] Yijun Han,[a] Can Li,[a] Sida Liu,[d] Xiaoyan Li,*[c] Guoqing Zhao*[a] and Yanyan Jiang*[ab]

Post-extraction, preventing the absorption of alveolar ridge to retain the supporting construction for implanted teeth is still a challenge. Herein, we developed modified chitosan (CS)-based hydrogel using *N*-hydroxysuccinimide-terminated 4-arm poly (ethylene glycol) (4-arm-PEG-NHS) as the crosslinking agent, after introducing it to the polyhexamethyleneguanidine hydrochloride (PHMB) solution, CS/PEG/PHMB hydrogel with the enhanced antibacterial properties was obtained. The CS/PEG hydrogel and CS/PEG/PHMB hydrogel prepared here showed excellent mechanical strength and their compressive strength could reach 440 kPa and 450 kPa, respectively. The composite hydrogel was designed to be directional porous, low cytotoxic, pH-sensitive, and degradable. The weight of the hydrogel was reduced by ∼30% after 28 days of incubation, and it swelled significantly in the acidic condition while it did not swell in the neutral and weakly alkaline environments, indicating an excellent biodegradability in the inflammation site. *In vitro* antibacterial experiments showed that the bacteriostatic rate of the CS/PEG/PHMB hydrogel against *S. aureus* was above 90%, which could effectively inhibit the spread of the bacteria and inflammation in the alveolar ridge. Additionally, the hybrid hydrogels demonstrated good biocompatibility with the NIH 3T3 fibroblast cells. Overall, the CS/PEG/PHMB hydrogel is a promising biological scaffold for maintaining the alveolar ridge and subsequently improving the success rate of the dental implant.

Received 17th August 2022
Accepted 27th October 2022

DOI: 10.1039/d2ra05151f

rsc.li/rsc-advances

1. Introduction

In stomatology, denture implantation is considered an effective approach to replacing missing teeth. In most cases, a dentist will recommend waiting for 3 to 6 months between tooth extraction and denture implantation to allow the extraction wound to fully heal.[1] During this period, the absorption of the alveolar ridge caused using the repair processes of soft and hard tissues at the extraction site will occur. Previous studies[2,3] have indicated that the absorption of the alveolar ridge is a normal and irreversible phenomenon after tooth extraction, and it directly affects the function and aesthetic effect of postoperative denture implant restoration. As tooth-supported construction, sufficient volume and favorable architecture of alveolar ridges are essential to obtain ideal functional and esthetic prosthetic reconstruction following implant therapy.[4] Generally, the amount of bone loss varies among different individuals and its mechanism is not clear yet. Some studies[5–8] have shown that the absorption of alveolar bone may be related to anatomical features, surgical procedures, and implant timing. The width and height of alveolar ridges can be lost by 50% within 6 months after tooth extraction,[9] and these changes in tissue contours at the extraction site would increase the difficulty of implant restoration. Alveolar Ridge Preservation (ARP) treatment is widely used in contemporary dental prosthetic practice, and there is reliable evidence to support its effectiveness.[10] The optimal condition of the alveolar ridge is to have sufficient width and height to provide support for the implant, and the application of biomaterials at the extraction site can maximize the preservation of bone mass and provide a good body condition for subsequent implant placement. Typically, the biomaterials used in alveolar ridge preservation include barrier membranes,[11] bioactive factors,[12] graft materials[13] and composite materials.[14] Barrier membranes can prevent soft tissues from growing into the extraction socket, but their poor mechanical strength make them easy to move and collapse. In

[a]*Key Laboratory for Liquid-Solid Structural Evolution & Processing of Materials (Ministry of Education), School of Materials Science and Engineering, Shandong University, Jinan, 250061, P. R. China. E-mail: guoqingzhao@sdu.edu.cn; yanyan.jiang@sdu.edu.cn*

[b]*Shenzhen Research Institute of Shandong University, Shenzhen, Guangdong, 518057, P. R. China*

[c]*Department of Endodontics, School and Hospital of Stomatology, Cheeloo College of Medicine, Shandong University & Shandong Key Laboratory of Oral Tissue Regeneration & Shandong Engineering Laboratory for Dental Materials and Oral Tissue Regeneration, Jinan, 250012, P. R. China. E-mail: lixiaoyanwhu@sdu.edu.cn*

[d]*Institute for Advanced Technology, Shandong University, Jinan, 250061, P. R. China*

† These authors contributed equally to this manuscript.

© 2022 The Author(s). Published by the Royal Society of Chemistry

Open Access Article. Published on 11 November 2022. Downloaded on 1/12/2026 3:45:44 PM.
This article is licensed under a Creative Commons Attribution-NonCommercial 3.0 Unported Licence.

recent years, bone graft materials have been of particular interest to the field of orthopedics because they are able to provide scaffolds for bone formation and preserve the space for bone growth. Compared with autogenous bone graft scaffolds, synthetic materials have the advantages that they do not involve selecting donors and the surgical wounds caused by them are smaller; therefore, they have less risk of disease transmission.[15] More importantly, the properties of these synthetic scaffolds can be easily adjusted according to the actual demands. The ideal scaffolds used for alveolar ridge preservation are supposed to show good biocompatibility, mechanical properties, and formability for irregularly shaped bone defects, as well as degradation rates matching bone growth.[16] One of the most commonly used synthetic scaffolds is a hydrogel. Hydrogels owning three-dimensional cross-linked network structures have physical and chemical properties similar to human tissues.[17] They can not only simulate the extracellular matrix (ECM) of bone but also allow the storage, and transport of various growth factors, cytokines, and nutrients due to their high permeability.[18–20] Hydrogels are typically grouped into natural and synthetic derivatives. Materials such as gelatin,[21] collagen,[22] chitosan,[23] alginate,[24] and hyaluronic acid[25] are natural products from the body or plants, and they are often used to fabricate hydrogels for use as scaffolds. Although natural materials can maintain many biological functions, they are limited in their application due to their poor mechanical properties.[26] Moreover, the natural materials are usually difficult to modify biochemically because they cannot be designed from the bottom-up like synthetic materials.[27] Synthetic hydrogels are often engineered from polymers like polyanhydrides,[28] polyaniline (PANI),[29] poly(vinyl alcohol) (PVA),[30] poly(ethylene glycol) (PEG)[31] and poly(ethylene oxide) (PEO).[32] These scaffolds are typically highly reproducible and simple to manufacture.[33] For these reasons, the development of a new natural/synthetic hybrid hydrogel scaffold is expected to combine the advantages of the above two types of hydrogels and overcome the existing drawbacks of conventional single-component stents, and it is considered a promising candidate to preserve the alveolar ridge and promote occlusal osteogenesis.

Chitosan (CS) is a natural, biodegradable polysaccharide derived by the deacetylation of chitin, the main component of the exoskeleton of crustaceans.[34] It has a natural inhibitory effect on the growth of a wide variety of bacteria.[35] Chitosan is soluble only in the acidic environment such as acetic, hydrochloric, and phosphoric acid solutions.[36] However, as a natural material, due to its low mechanical strength and limited manufacturing capabilities, chitosan is difficult process into a hydrogel that has controlled physical and chemical properties to meet specific applications. Since natural/synthetic composites can cover these shortages of natural polymers, chitosan-based hybrid hydrogels have found plenty of applications in the medical field over the past few decades.[37–39] During the preparation of these hydrogels, chemical cross-linking strategies are usually chosen instead of physical cross-linking strategies,[40] to fabricate a more stable structure of hydrogels with great mechanical strength. Multi-arm PEG is one of the commonly used chemical crosslinking agents in hydrogel systems. PEG is an amphiphilic polyether diol that can be dissolved in water and organic solvents.[36] It is low immunogenic, non-toxic, and has been approved by Food and Drug Administration (FDA, USA) for various biomedical applications.[41] Moreover, the terminal part of multi-arm PEG can be easily functionalized with numerous reactive groups such as amino, vinyl, thiol, and carboxyl to allow different types of reactions, making it utilized extensively as a soluble polymeric modifier in organic synthesis.

Nowadays, hydrogels are being gradually applied in dental studies.[42–44] It is worthwhile to develop an optimized hydrogel that can be implanted into the tooth extraction area for the use of alveolar ridge preservation. The objective of this study was to synthesize and characterize a chitosan-based hydrogel cross-linked by *N*-hydroxysuccinimide-terminated 4-arm PEG (4-arm-PEG-NHS) and explore the potential of the composite hydrogel as a biological scaffold for alveolar ridge promotion. As for the functional group to form the covalent cross-linking bond, the NHS group was chosen since the condensation reaction between the NHS end group of the 4-arm PEG and the primary amine group of chitosan proceeds with high selectivity without adding other reagents.[45] Hydrogels synthesized *via* this chemical crosslinking method have been applied clinically as sealants to stop fluid leaks in neurological and ophthalmic surgery.[46] Further, the hydrogel prepared here was modified using sodium hydroxide to obtain higher mechanical strength. It should also be noted that, even with the high levels of sterility common to the operating theater, a small number of bacteria introduced to the implant site could be problematic given the altered host immune response that exists at the wound site.[47] Besides, drug resistance can be produced so rapidly in antibiotic treatment that new antibacterial methods should be tried to replace the traditional drug treatment. To address these potential problems, the hydrogels that display antibacterial activity has been designed here. In addition to choosing chitosan which has antibacterial properties as the matrix, polyhexamethyleneguanidine hydrochloride (PHMB) was also added to the hydrogel system as an antimicrobial biocide. PHMB is composed of repeating basic biguanidine units connected by hexamethylene hydrocarbon chains and its bactericidal properties have been proven against a range of species.[48] The micromorphology, degradability, mechanical strength, bacteriostatic performance, and cytotoxicity of the composite hydrogels were studied separately. The results showed that the CS/PEG/PHMB hydrogel would make promising bio-scaffold material used to preserve the alveolar ridge for clinical implantation.

2. Experimental section

2.1. Materials

Chitosan (the degree of deacetylation was 75–85%) was purchased from Sigma-Aldrich (China). 4-Arm-PEG-*N*-hydroxysuccinimide (4-arm-PEG-NHS, M_w 10 000) was purchased from Ruixibio (Ruixi Biological Technology, Xi'an, China). Acetic acid was purchased from SINOPHARM (Sinopharm Chemical Reagent Co., Ltd, China). Polyhexamethyleneguanidine

 © 2022 The Author(s). Published by the Royal Society of Chemistry

Open Access Article. Published on 11 November 2022. Downloaded on 1/12/2026 3:45:44 PM.
This article is licensed under a Creative Commons Attribution-NonCommercial 3.0 Unported Licence.

hydrochloride (PHMB), eosin Y water solution, sodium acetate trihydrate, and sodium hydroxide were purchased from Macklin (Macklin Biochemical Co., Ltd, Shanghai, China). Phosphate buffer saline (PBS) was purchased from Yuanye (Yuanye Bio-Technology Co., Ltd, Shanghai, China). NIH 3T3 cells were obtained from the Cell Bank of Type Culture Collection (Chinese Academy of Sciences, Shanghai, China). Unless stated otherwise, all reagents and solvents were of biological grade and were used without further purification.

2.2. Synthesis of CS/PEG hydrogel

CS/PEG hydrogel was prepared as follows. 100 mg of chitosan was dissolved in 10 mL of 1% (v/v) acetic acid solution, then heated to 60 °C in a water bath and stirred at 200 rpm until chitosan was dissolved completely. The chitosan solution was filtered using 1000 mesh nylon microporous membrane and its pH was adjusted to 6 using sodium hydroxide. Then, 10 mg of 4-arm-PEG-NHS was added to 1 mL of chitosan solution in a centrifuge tube and the illiquid hydrogel would be formed in 10 minutes with ultrasonic treatment at room temperature. The hydrogel was allowed to stand for an additional 50 minutes to ensure that the crosslink net within it was completely fabricated. Afterward, 1 mL of 5% (w/v) sodium hydroxide solution was slowly added to the top of the gel, followed by 1 h standing. The synthesized product was dialyzed against ultrapure water for 12 h to remove small molecules like sodium hydroxide from the hydrogel.

2.3. Synthesis of CS/PEG/PHMB hydrogel

The synthesis of CS/PEG/PHMB hydrogel was similar to that described previously. Briefly, the chitosan was dissolved in an acetic acid solution completely and then filtered; its pH was adjusted to 6 with the addition of sodium hydroxide. Subsequently, the solution was transferred into a 24-well plate (1 mL per well) and divided into three groups. 4-Arm-PEG-NHS (10 mg per well) and a range of concentrations of PHMB (0, 0.3, 1% w/v) were added into the well groups. After 10 minutes of ultrasonic and 50 minutes of standing, 5% (w/v) sodium hydroxide solution was added to the plate (1 mL per well) followed by 1 h of standing. The synthesized products were dialyzed against ultrapure water for 12 h to be neutral.

2.4. Morphology and structure characterization of the hydrogels

The chemical structure of 4-arm-PEG-NHS cross-linked chitosan hydrogel was analyzed using FTIR spectroscopy (BRUKER OPTICS, TENSOR37, Switzerland). The hydrogel was freeze-dried to a constant weight before the sample preparation. The micromorphology of CS/PEG hydrogel and CS/PEG/PHMB hydrogel was analyzed using SEM (COXEM, EM-30+, Korea). Hydrogels were freeze-dried and stuck on the sample stage with conductive tape, then sputter-coated with gold using an ion sputtered under a high vacuum. The acceleration voltage was set at 10–15 kV and the morphology of the hydrogels was examined.

2.5. Degradation test of hydrogels

Hydrogels were placed in 20 mL of PBS at various pH (pH = 5.5, 6.5, 7.5) and incubated at 70 °C and 37 °C to observe the accelerated degradation and actual time degradation behavior. During the degradation process, hydrogels were removed at respective time points, washed 3 times with ultra-pure water, and then weighed wet after absorbing the moisture on the surface. *In vitro* degradation ratio was calculated using the following equation:

$$D_r = (W_0 - W_t)/W_0$$

where D_r is the degradation ratio and W_0 and W_t are the initial weights of samples and wet weights of samples after incubation, respectively. To determine the PHMB loss during gel degradation, in the experimental part of the antibacterial hydrogels, 10 mL of soaking solution was taken out at each test time point, followed by replenishing 10 mL of fresh PBS into the vessel. The UV-Vis absorption of the solution was detected using a UV-Vis spectrophotometer (Analytik Jena AG, SPECORD 200 PLUS, Germany) as reported before.[49] All experiments were repeated three times.

2.6. Mechanical property testing of hydrogels

The compressive properties of CS/PEG hydrogel and CS/PEG/PHMB hydrogel were tested using a universal testing machine WDW-100. The samples were prepared in 7 mm high and 8 mm in diameter. The loading rate was 10 mm min^{-1} and the maximum compression deformation rate was set at 80%.

2.7. *In vitro* antibacterial experiments

The bacteriostatic circle test with *S. aureus* (ATCC 25923) model were performed to investigate the antibacterial performance of CS/PEG/PHMB hydrogels. *S. aureus* was incubated in BHI media at 37 °C for 24 h. The activated bacterial solutions (1.0×10^8 CFU per mL) were diluted ten times before use. The hydrogels were cut into small round pieces with uniform size (10 mm in diameter) and cultured with the bacterial suspension on BHI agar at 37 °C for 24 h. Finally, the bacteriostatic rings were observed and the width of the bacteriostatic circle was calculated according to the following equation:

$$H = (D - d)/2$$

where D and d represent the outside and inside diameters of the bacteriostatic circle, respectively. The morphology and biomass volume of the bacteria cultured with hydrogels was observed using SEM. The anti-adhesion and anti-biofilm tests were also performed. 1 mL of the diluted bacterial suspension was incubated with CS/PEG/PHMB hydrogels in a biochemical incubator at 37 °C for 24 h. The samples were washed with PBS to remove any non-adherent bacteria after incubation. Then, the adhered bacteria were subjected to 20 min of ultrasonic treatment, followed by 2 min of vortex in 5 mL of PBS. Finally, 20 μL of diluted bacterial suspension was coated and incubated on BHI agar overnight at 37 °C. The number of bacterial colonies on the

Open Access Article. Published on 11 November 2022. Downloaded on 1/12/2026 3:45:44 PM.
This article is licensed under a Creative Commons Attribution-NonCommercial 3.0 Unported Licence.

plates was recorded using ImageJ. All experiments were repeated three times. The antibacterial rate was calculated using the following equation:

$$\text{Antibacterial rate } (\%) = \frac{N_c - N_s}{N_c} \times 100\%$$

where N_c and N_s correspond to the number of bacteria colonies on the control CS/PEG hydrogel and CS/PEG/PHMB hydrogel, respectively.

2.8. Cytotoxicity studies

The cytotoxicity of CS/PEG/PHMB hydrogel to mammalian cells was evaluated using the cell counting kit-8 (CCK-8) and live/dead cell staining experiments, using NIH 3T3 fibroblast cells as the model. Briefly, NIH 3T3 cells in the logarithmic growth period were seeded into a 24-well plate with the cell culture medium and the density of the cell suspension was 8×10^3 cells per well. The plate was cultured at 37 °C for 24 h. Subsequently, the cells were cultured with CS/PEG/PHMB hydrogels at various concentrations of PHMB (0, 0.3, and 1% w/v) in the medium for 24 h and 48 h. After that, the culture medium was replaced with CCK-8 solution (350 μL per well, containing 10% CCK-8 reagent) and the cells were incubated for an additional 1 h. Finally, the sample solution was transferred into a 96-well plate (100 μL per well) and its absorbance was detected at 450 nm using a microplate reader. In addition, the cells co-cultured with hydrogels were stained using NucGreen and propidium iodide (PI) and scanned using a fluorescence microscope. NucGreen was utilized to stain the live cells in green, while PI stained the dead cells in red. The staining process lasted for 1–2 h and then the cells were observed using a fluorescence microscope. All experiments were repeated three times.

3. Results and discussion

3.1. Synthesis and characterization of the hydrogels

4-Arm-PEG-NHS was grafted onto chitosan by coupling the NHS end group to the primary amino group of chitosan to form an amide bond and the optimal reaction condition is pH 7–9. It is worth mentioning that the hydrolysis of NHS esters and the reaction of NHS esters with primary amines are competitive, and the hydrolysis rate of NHS esters increases with the increasing pH of the solution. Therefore, the reaction environment of chitosan and 4-arm-PEG-NHS was selected to be weakly acidic (pH = 6) to ensure the high efficiency of the gel-forming reaction. The reaction mechanism and implantation procedure

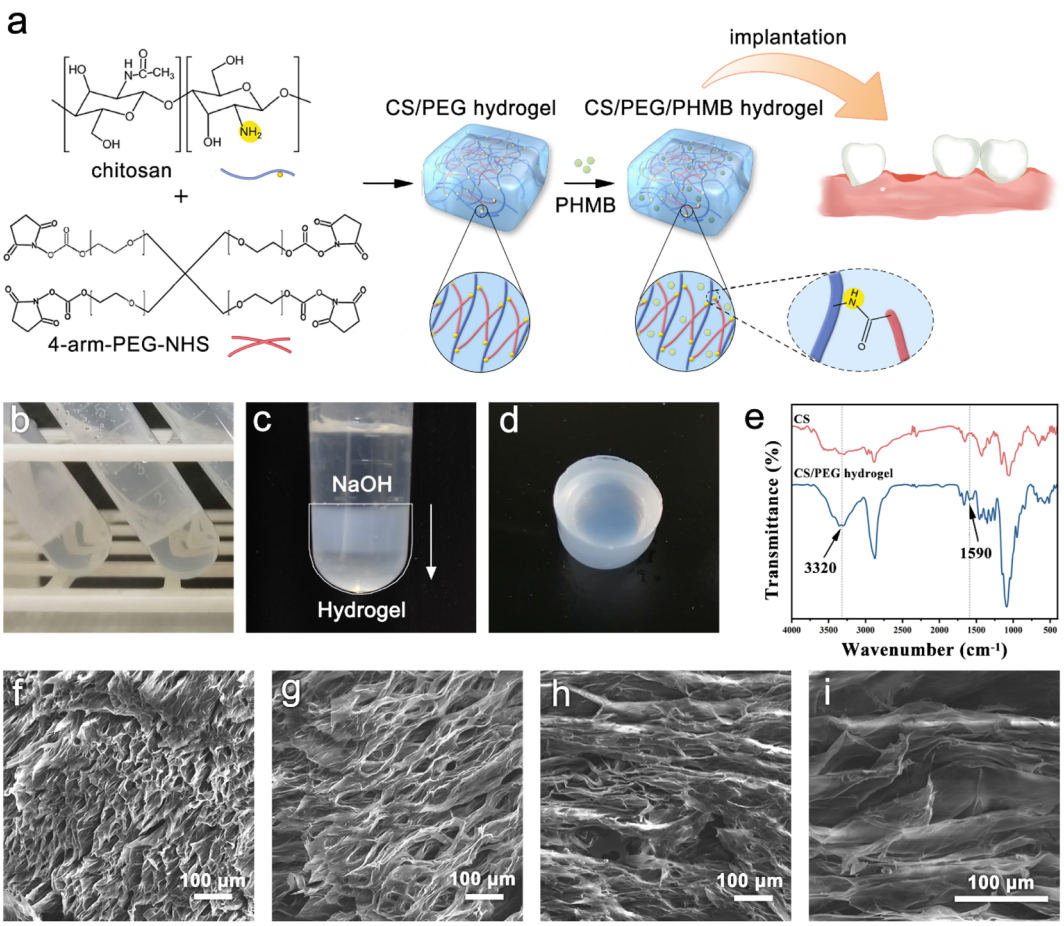

Fig. 1 Preparation and characterization of CS/PEG hydrogel and CS/PEG/PHMB hydrogel. (a) Schematic illustration for the preparation of CS/PEG hydrogel and CS/PEG/PHMB hydrogel and their application for alveolar ridge preservation. (b–d) Images of CS/PEG hydrogel. (e) FTIR spectra of chitosan and CS/PEG hydrogel. (f–i) SEM images of CS/PEG hydrogel and CS/PEG/PHMB hydrogel.

 © 2022 The Author(s). Published by the Royal Society of Chemistry

Open Access Article. Published on 11 November 2022. Downloaded on 1/12/2026 3:45:44 PM.
This article is licensed under a Creative Commons Attribution-NonCommercial 3.0 Unported Licence.

of the hydrogel are illustrated in Fig. 1a. The crosslinking reaction between primary amino groups and amine-reactive hydroxysuccinimide esters is known to bring about rapid, homogeneous, and biocompatible polymerization at ambient conditions, and it has been applied many times in clinical applications.[50] The gelation occurred within 10 minutes after the addition of 4-arm-PEG-NHS crosslinker, and the presented product was colorless, transparent, and had no fluidity (Fig. 1b). However, since the degradation rate of chitosan molecules is fast in an acidic environment, the hydrogel lacking sufficient mechanical strength cannot be removed from the container without damage. Thus, sodium hydroxide solution was used in the hydrogel modification to improve its mechanical property. The protonated amino groups within chitosan were neutralized by alkali treatment and the ion repulsion between polymer chains was eliminated. Meanwhile, the intermolecular hydrogen bonds, chitosan microcrystals, and hydrophobic interactions were retained. After adding the alkali dropwise, the appearance of the hydrogel turned from colorless transparent to milky white from top to bottom (Fig. 1c), and its mechanical strength was improved greatly during this process, which allowed the hydrogel to be removed intact from the centrifuge tube without breaking. The surface of the chitosan-based hydrogel prepared using this method was smooth, as shown in Fig. 1d. Moreover, the hydrogels have *in situ* formability, which permits a homogeneous encapsulation of drugs,[51] and is helpful for them to be prepared into the required shapes to meet the needs of filling the extraction sockets. Successful formation of the crosslinking structure in the CS/PEG hydrogel was confirmed using Fourier transform-infrared (FTIR) spectroscopy, as shown in Fig. 1e. There was a new peak appearing in the spectrum of CS/PEG hydrogel at 1590 cm^{-1}, which was the amide II band correlated to the bending vibration of N–H.[52,53] The absorption peak occurring at 3320 cm^{-1} was the amide A band ascribed to the stretching vibration of N–H and its intensity enhanced compared with that of chitosan, suggesting that the number of amide bonds in the CS/PEG hydrogel increased with the proceeding of the crosslinking reaction and that its intensity was affected by the crosslinking degree.[23,54] Furthermore, the peaks at 1809, 1781, and 1739 cm^{-1} are characteristic absorptions of NHS ester within PEG[55] and they cannot be found in the spectrum of CS/PEG hydrogel, indicating that the 4-arm-PEG-NHS had reacted with NH_2 groups within chitosan by acylation. Thus, the formation of the –NH–C═O– structure in the cross-linked hydrogel was confirmed. After the verification of the successful synthesis of CS/PEG hydrogel, the hydrogel possessing antibacterial properties was further developed. PHMB powder was added to the precursor polymer solution before crosslinking to obtain CS/PEG/PHMB hydrogel. The morphological analysis of CS/PEG hydrogel and CS/PEG/PHMB hydrogel was performed using a scanning electron microscope (SEM) (Fig. 1f–i). The hydrogels were freeze-dried and then analyzed in the longitudinal section (paralleling the gel-forming direction in Fig. 1c) and cross-section respectively. It can be observed that the longitudinal section of the hydrogel (Fig. 1f and g) showed a homogeneous, porous three-dimensional directional network structure with a pore size ranging from 15 μm to 30 μm, and the porosity was 33.18% calculated using ImageJ. The porous structure of hydrogels can simulate ECM, which is advantageous to the proliferation, differentiation, and gene expression of stem cells in bone regeneration.[56,57] In contrast, the cross-section of hydrogels presented lamellar structures, as shown in Fig. 1h and i, demonstrating that the hydrogels prepared here were anisotropic. Hydrogels with anisotropic structures and appropriate mechanical properties are similar to biological tissues,[58] and the anisotropic micropatterns were demonstrated to directionally induce cell alignment and accelerate cell migration,[59] which is vital for constructing osteogenic microenvironment *in vivo*.[60]

3.2. *In vitro* degradation of hydrogels

The degradability of the hydrogel is an important parameter to be considered for the application of bone tissue repair and regeneration. Ideally, the hydrogel is supposed to degrade neither too slowly nor too quickly in order to provide an appropriate time for tissue ingrowth. In this study, the hybrid hydrogel was applied to fill the socket after extraction to ensure that there were adequate alveolar bones to provide support for the subsequent dental implant. Meanwhile, the hydrogel was expected to be fully degraded during the interval of tooth implantation hence the secondary removal of implants can be avoided. Therefore, the degradation properties of CS/PEG hydrogel and CS/PEG/PHMB hydrogel were investigated (Fig. 2). The samples were placed in phosphate-buffered saline (PBS) at various pH and incubated at 70 °C and 37 °C to observe the accelerated degradation and actual time degradation behavior. In the accelerated degradation experiment (Fig. 2a and b), one can easily find that the degradation behavior of CS/PEG hydrogel was sensitive to pH value. A significant swelling on CS/PEG hydrogel was observed in the simulated environment of pH 5.5, and its weight increased by 103.47% after 2 days of incubation at 70 °C, which exhibited the application potential in load and sustained release of drug and growth factor. In contrast, the mass and volume loss occurred in hydrogels in an environment of pH 6.5 and 7.5, and the state and mechanical strength of the hydrogels were kept stable as shown in Fig. 2a, which was favorable for providing steady support for the alveolar ridge during the degradation process. At the two pH values, the degradation ratio of CS/PEG hydrogel reached 29.83% and 30.39% under the incubation at 37 °C after 28 days. Considering the experimental errors, we could say that the degradation behavior of CS/PEG hydrogel showed the same pattern at pH 6.5 and 7.5. Similarly, the degradation ratio of CS/PEG/PHMB hydrogel reached ∼37% after 28 days of incubation at 37 °C (Fig. 2d). The *in vitro* degradation experiments revealed that the hydrogels had appropriate degradation time to afford space for new bone formation, and were capable of supporting the long-term growth and proliferation of osteogenic stem cells.[61] Moreover, approximately, only 2.1% and 1.8% of the loaded PHMB were released from the CS/PEG/PHMB hydrogels during degradation at pH 6.5 and 7.5 after 28 days, respectively (Fig. 2e). In other words, more than 97% of the loaded PHMB was retained in the hydrogels, indicating that the CS/PEG/

Open Access Article. Published on 11 November 2022. Downloaded on 1/12/2026 3:45:44 PM.
This article is licensed under a Creative Commons Attribution-NonCommercial 3.0 Unported Licence.

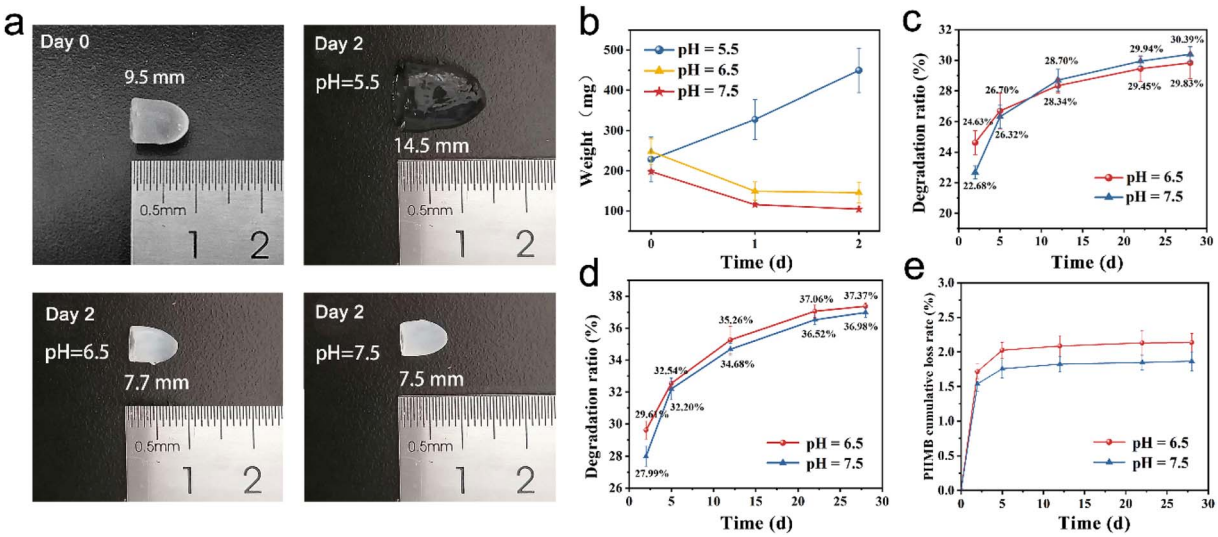

Fig. 2 *In vitro* degradation properties of CS/PEG hydrogel and CS/PEG/PHMB hydrogel. (a) Photographs of CS/PEG hydrogels in accelerated degradation experiments. (b) CS/PEG hydrogel mass change curves after incubation at 70 °C for 2 days. (c) *In vitro* degradation ratio of CS/PEG hydrogels after incubation at 37 °C for 28 days. (d) *In vitro* degradation ratio of CS/PEG/PHMB hydrogels after incubation at 37 °C for 28 days. (e) The cumulative loss rate of PHMB in degradation experiments. The data shown was ±SD and these experiments were repeated 3 times.

PHMB hydrogels could maintain the excellent antibacterial property during the whole degradation process, which would avoid the occurrence of inflammation and provide a good biological environment for wound healing at the extraction socket.

3.3. Mechanical properties of the hydrogels

Compression tests were performed to investigate the mechanical strength of CS/PEG hydrogel and CS/PEG/PHMB hydrogel. The samples were prepared 7 mm high and 8 mm in diameter and compressed using the universal testing machine. The compressive stress–strain curves of the hydrogels are shown in Fig. 3. Generally, the appropriate mechanical strength of hydrogels can imitate the osteogenic differentiation of stem cells in the osteogenic micro-environment.[62] It can be seen from the curves that irreversible damage occurred in the CS/PEG hydrogel under maximum compression of 440 kPa with a strain of 56.45%. Similarly, the CS/PEG/PHMB hydrogel was damaged under maximum compression of 450 kPa with a strain of 66.40%. Compared with the previous study[63] in which the chitosan-based hydrogel possessed a compressive strength of 210 kPa, the hydrogels we designed exhibit more advantageous mechanical strength and toughness, which is significant for the support of alveolar ridge around the extraction socket and can imitate the proliferation of periodontal tissue meanwhile.[64,65] The above results indicate that the CS/PEG hydrogel and CS/PEG/PHMB hydrogel are promising bioscaffolds for alveolar ridge preservation.

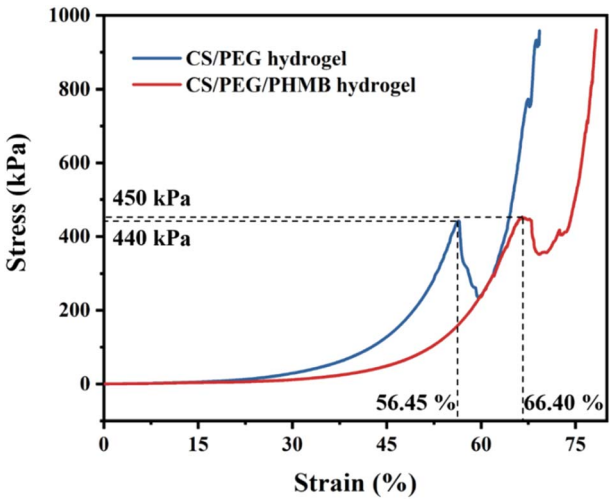

Fig. 3 Stress–strain curves of CS/PEG hydrogel and CS/PEG/PHMB hydrogel.

3.4. *In vitro* antibacterial activities of the hydrogels

Among several crucial considerations for the implantation of a biomaterial, the main concern is the introduction of infection. Biomaterial-centered infections are common, accounting for about 45% of all nosocomial infections.[47] The infection would lead to slowed tissue regeneration around the implant site, and in some extreme cases, the implant must be removed. Therefore, the design and synthesis of hydrogels with antibacterial activity as scaffolds for tissue engineering are highly anticipated.[66] Herein, we developed CS/PEG/PHMB hydrogels whose surfaces are antibacterial. The antibacterial effects of these hydrogels were assessed by the bacteriostatic circle assay with *S. aureus* as the model. The infectious complications after tooth extraction such as dry socket and bacteremia are usually a Gram-positive coccus infection mixed with the Gram-negative bacillus. Considering the homoplasy of Gram-positive cocci such as morphological characteristics and pathogenic mechanisms, *S. aureus* was selected to be a representative of Gram-

 © 2022 The Author(s). Published by the Royal Society of Chemistry

Open Access Article. Published on 11 November 2022. Downloaded on 1/12/2026 3:45:44 PM.
This article is licensed under a Creative Commons Attribution-NonCommercial 3.0 Unported Licence.

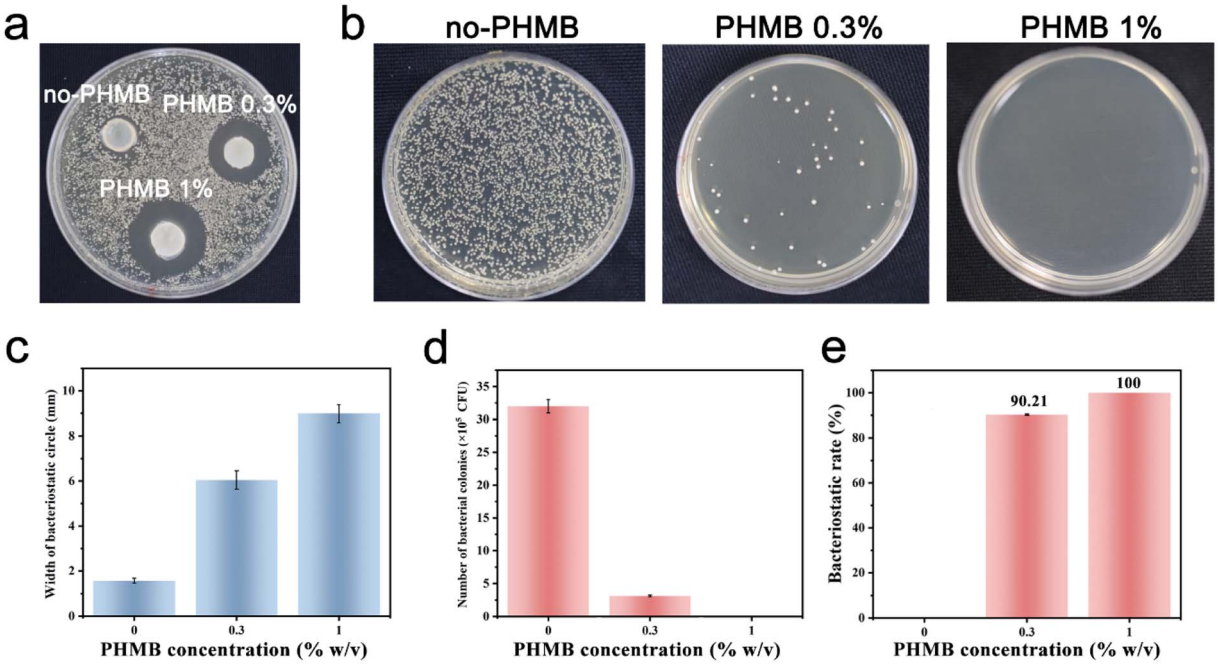

Fig. 4 Antibacterial properties of CS/PEG/PHMB hydrogels. (a) Photograph of bacteriostatic circles of CS/PEG/PHMB hydrogels loaded with different concentrations of PHMB after incubation with *S. aureus* for 24 h. (b) Photographs of the colonies of *S. aureus*. (c) Width of bacteriostatic circles of CS/PEG/PHMB hydrogels. (d) Numbers of bacterial colonies of different samples. (e) Antibacterial efficiency of the samples against *S. aureus*. The data represent mean ± SD and these experiments were repeated 3 times.

positive coccus for the preliminary study. The hydrogels were cut into small round pieces of uniform size and cultured with *S. aureus* suspension on Brain Heart Infusion (BHI) agar for 24 h. Then the bacteriostatic rings were observed and the width of the bacteriostatic circle was calculated. As shown in Fig. 4a, there was no obvious antibacterial circle around CS/PEG hydrogel, while conspicuous bacteriostatic circles were observed around the CS/PEG hydrogels encapsulated with PHMB (0.3% and 1%), and the inhibition zones of PHMB 1% samples were visibly larger than that of 0.3% ones. The widths of bacteriostatic circles of CS/PEG hydrogel, and CS/PEG/PHMB 0.3% and 1% hydrogels were 1.56 mm ± 0.1 mm, 6.04 mm ± 0.4 mm and 9.00 mm ± 0.4 mm, respectively (Fig. 4c), suggesting that the antibacterial properties of hydrogels were greatly improved with the addition of PHMB. Next, the number of bacterial colonies on the surfaces of CS/PEG/PHMB hydrogels was counted after ultrasonic concussion and 10^3 × dilution treatment. Fig. 4b and d clearly show that the CS/PEG/PHMB 0.3% hydrogel was already able to kill most of the bacteria with a bacteriostatic rate above 90% (Fig. 4e), and no bacterial colonies were observed on

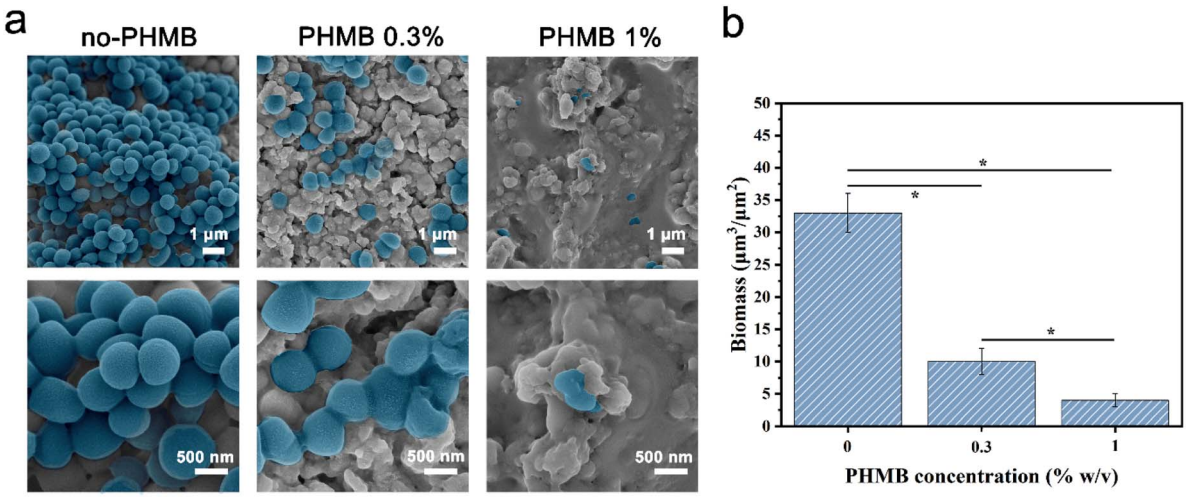

Fig. 5 (a) SEM images of *S. aureus* cells on the surfaces of CS/PEG hydrogel and CS/PEG/PHMB hydrogel after incubation of 24 h. (b) Biomass volume per area of the hydrogel surface. The data shown was ±SD and these experiments were repeated 3 times. *p < 0.05.

Open Access Article. Published on 11 November 2022. Downloaded on 1/12/2026 3:45:44 PM.
This article is licensed under a Creative Commons Attribution-NonCommercial 3.0 Unported Licence.

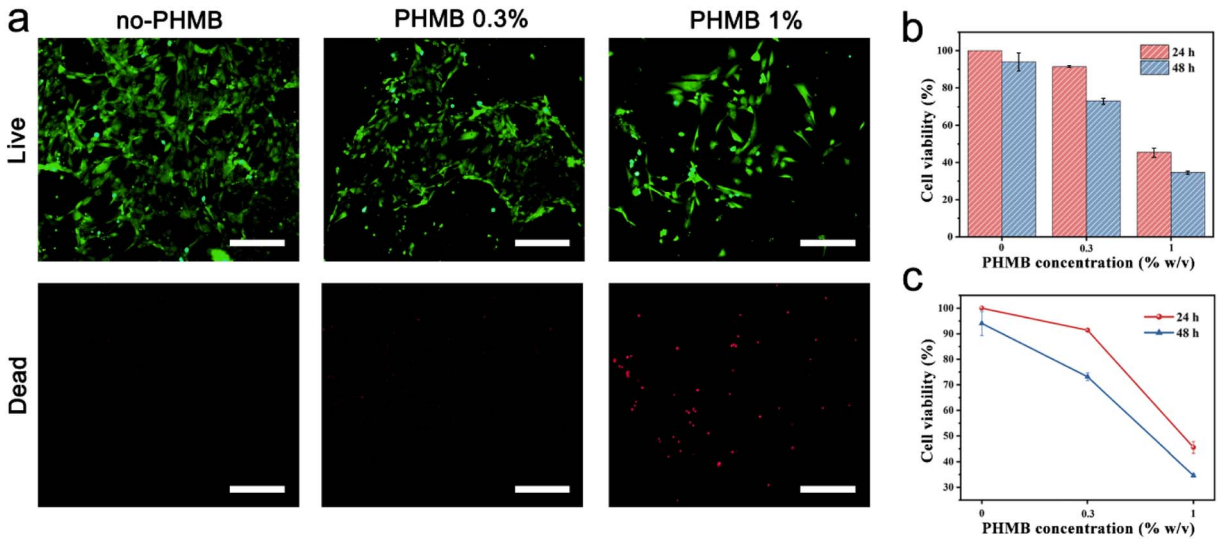

Fig. 6 Cytotoxicity of CS/PEG hydrogel and CS/PEG/PHMB hydrogel. (a) Fluorescence microscopy images of NIH 3T3 cells after incubation with CS/PEG hydrogel and CS/PEG/PHMB hydrogel for 24 h (corresponding scale bars were 200 μm). (b and c) Cell viabilities of NIH 3T3 cells after incubation with different samples for 24 h and 48 h. The data shown was ±SD and these experiments after 3 repetitions.

the plate of the PHMB 1% group, which means the bacteriostatic rate of CS/PEG/PHMB 1% hydrogel was up to 100%. The data showed that CS/PEG/PHMB hydrogels were capable of inhibiting *S. aureus* proliferation effectively.

To visualize the bactericidal effects of the hydrogels, SEM was used to observe the morphologies and membrane integrity of the bacteria incubated with different samples (Fig. 5a). The structure of bacterial cells on the surface of the CS/PEG hydrogel was observed to remain almost intact. As expected, SEM images show that the inhibitory activity of the hydrogel surface apparently increased with the introduction of PHMB. Most cells on the surface of CS/PEG/PHMB 0.3% hydrogel were shriveled and cracked, while only a few parts of them maintained complete cell walls. On the surface of CS/PEG/PHMB 1% hydrogel, nearly all cells exhibited considerable damage and no structure of biofilm was observed, indicating a higher bactericidal efficacy of the hydrogel with the increase of PHMB content. Additionally, compared with the CS/PEG hydrogel, the number of bacteria cells on the surfaces of PHMB 0.3% and 1% hydrogels decreased significantly, as shown in Fig. 5b. The total biomass on the surface of CS/PEG/PHMB 0.3% hydrogel decreased to almost a third of that of the CS/PEG hydrogel, while the PHMB 1% ones decreased to about one-eighth of that. The data demonstrated that the CS/PEG/PHMB hydrogel can not only inactivate bacteria effectively but also possess the ability to resist bacterial adhesion. As an implantable scaffold material, the CS/PEG/PHMB hydrogel with advantageous antibacterial activity can protect the extraction socket from being infected, thus this optimized hydrogel is appropriate for alveolar ridge preservation.

3.5. Cytotoxicity studies

It is well known that good biocompatibility and biosafety of implantable scaffold materials are necessary for tissue engineering.[67] The cytotoxicity of the CS/PEG hydrogel and CS/PEG/PHMB hydrogel to mammalian cells was evaluated *via* CCK-8 and live/dead cell staining experiments using NIH 3T3 cells as the model. As shown in Fig. 6a, almost no dead cells were observed after incubation with CS/PEG hydrogel and CS/PEG/PHMB 0.3% hydrogel for 24 h. Meanwhile, according to the data of the CCK-8 experiments (Fig. 6b), 100% and 94.04% of NIH 3T3 cells remained viable after incubating with CS/PEG hydrogel for 24 h and 48 h, respectively. This demonstrated the good biocompatibility and low cytotoxicity of CS/PEG hydrogel toward NIH 3T3 cells. Compared with the CS/PEG hydrogel group, the cell viability decreased to 91.39% and 73.16% after incubating with CS/PEG/PHMB 0.3% hydrogel for 24 h and 48 h, respectively, suggesting that the cytotoxicity of the hydrogel increased slightly with the addition of PHMB. According to ISO10993, the CS/PEG/PHMB 0.3% hydrogels exhibited an acceptable effect on the cell viability after incubation of 24 h or 48 h. But the cell viability decreased to 45.50% and 34.62% after incubation for 24 h and 48 h, respectively, when the PHMB concentration among hydrogel increased to 1%. The results revealed that the cytotoxicity of hydrogels clearly had a positive correlation with the content of PHMB (Fig. 6c). For future clinical applications, more precise concentration and administration frequency should be confirmed to enhance the hydrogel to obtain better bactericidal performance and biocompatibility.

4. Conclusions

In this study, a 4-arm-PEG-NHS cross-linked chitosan hydrogel was designed to be a degradable biological scaffold material for alveolar ridge preservation. The covalently cross-linked hydrogel was fabricated *via* the primary amine ester reaction under physiological conditions and was further loaded with PHMB to

 © 2022 The Author(s). Published by the Royal Society of Chemistry

Open Access Article. Published on 11 November 2022. Downloaded on 1/12/2026 3:45:44 PM.
This article is licensed under a Creative Commons Attribution-NonCommercial 3.0 Unported Licence.

improve its antibacterial property. CS/PEG hydrogel prepared here had pH-responsive swelling properties and it swelled significantly in the acidic condition. In an environment of weak acid and neutral alkalinity, the volume of the hydrogel shrank. The as-prepared hydrogel possessed superior mechanical strength with the compressive strength of 440 kPa, which provides a significant advance over materials reported before. *In vitro* degradation experiments indicated that CS/PEG hydrogel and CS/PEG/PHMB hydrogel both had appropriate rates of degradation. Additionally, the antibacterial performance of CS/PEG hydrogel was significantly enhanced by introducing PHMB into this network system. CS/PEG/PHMB hydrogel exhibited excellent antibacterial ability and was capable of inhibiting the growth and adhesion of bacteria effectively. Moreover, cell experiments showed that the CS/PEG hydrogel and CS/PEG/PHMB hydrogel possessed good biocompatibility and low cytotoxicity toward mammalian cells. Overall, the CS/PEG/PHMB hydrogel is an ideal scaffold material for osteogenic application and is expected to be used as a new candidate for alveolar ridge preservation in dental surgery, and it also provides a new strategy for bone defect restoration in the clinic.

Conflicts of interest

There are no conflicts to declare.

Acknowledgements

The authors acknowledge financial support from the National Natural Science Foundation of China (Grant No. 52101287 and U1806219), the Shenzhen Fundamental Research Program (JCYJ20190807092803583), Shandong Provincial Natural Science Foundation (No. ZR2020MH191) and the Natural Science Foundation of Jiangsu Province (Grant No. BK20190205). The Special Funding also supports this work in the Project of the Qilu Young Scholar Program of Shandong University.

References

1 L. Wang, L. Zheng, C. Li, S. Dong, A. Lan and Y. Zhou, Adrenomedullin delivery in microsphere-scaffold composite for remodeling of the alveolar bone following tooth extraction: an experimental study in the rat, *Biomed. Eng.*, 2013, **12**, 99.

2 A. Barone, M. Ricci, P. Tonelli, S. Santini and U. Covani, Tissue changes of extraction sockets in humans: a comparison of spontaneous healing *vs.* ridge preservation with secondary soft tissue healing, *Clin. Oral Implants Res.*, 2013, **24**, 1231–1237.

3 R. E. Jung, A. Philipp, B. M. Annen, L. Signorelli, D. S. Thoma, C. H. Hammerle, T. Attin and P. Schmidlin, Radiographic evaluation of different techniques for ridge preservation after tooth extraction: a randomized controlled clinical trial, *J. Clin. Periodontol.*, 2013, **40**, 90–98.

4 R. Schneider, Prosthetic concerns about atrophic alveolar ridges, *Postgrad. Dent.*, 1999, **6**, 3–7.

5 S. Spinato, P. Galindo-Moreno, D. Zaffe, F. Bernardello and C. M. Soardi, Is socket healing conditioned by buccal plate thickness? A clinical and histologic study 4 months after mineralized human bone allografting, *Clin. Oral Implants Res.*, 2014, **25**, e120–e126.

6 S. Fickl, O. Zuhr, H. Wachtel, W. Bolz and M. Huerzeler, Tissue alterations after tooth extraction with and without surgical trauma: a volumetric study in the beagle dog, *J. Clin. Periodontol.*, 2008, **35**, 356–363.

7 H. M. Alharbi, N. Babay, H. Alzoman, S. Basudan, S. Anil and J. A. Jansen, Bone morphology changes around two types of bone-level implants installed in fresh extraction sockets–a histomorphometric study in Beagle dogs, *Clin. Oral Implants Res.*, 2015, **26**, 1106–1112.

8 S. Engelhardt, P. Papacosta, F. Rathe, J. Ozen, J. A. Jansen and R. Junker, Annual failure rates and marginal bone-level changes of immediate compared to conventional loading of dental implants. A systematic review of the literature and meta-analysis, *Clin. Oral Implants Res.*, 2015, **26**, 671–687.

9 C. Sbordone, P. Toti, R. Martuscelli, F. Guidetti, L. Ramaglia and L. Sbordone, Retrospective volume analysis of bone remodeling after tooth extraction with and without deproteinized bovine bone mineral insertion, *Clin. Oral Implants Res.*, 2016, **27**, 1152–1159.

10 F. Vignoletti, P. Matesanz, D. Rodrigo, E. Figuero, C. Martin and M. Sanz, Surgical protocols for ridge preservation after tooth extraction. A systematic review, *Clin. Oral Implants Res.*, 2012, **23**(Suppl 5), 22–38.

11 D. Carmagnola, P. Adriaens and T. Berglundh, Healing of human extraction sockets filled with Bio-Oss, *Clin. Oral Implants Res.*, 2003, **14**, 137–143.

12 A. C. Carreira, F. H. Lojudice, E. Halcsik, R. D. Navarro, M. C. Sogayar and J. M. Granjeiro, Bone morphogenetic proteins: facts, challenges, and future perspectives, *J. Dent. Res.*, 2014, **93**, 335–345.

13 G. Serino, S. Biancu, G. Iezzi and A. Piattelli, Ridge preservation following tooth extraction using a polylactide and polyglycolide sponge as space filler: a clinical and histological study in humans, *Clin. Oral Implants Res.*, 2003, **14**, 651–658.

14 C. Maiorana, P. P. Poli, M. Deflorian, T. Testori, F. Mandelli, H. Nagursky and R. Vinci, Alveolar socket preservation with demineralised bovine bone mineral and a collagen matrix, *J. Periodontal Implant Sci.*, 2017, **47**, 194–210.

15 T. D. Borg and B. L. Mealey, Histologic healing following tooth extraction with ridge preservation using mineralized *versus* combined mineralized-demineralized freeze-dried bone allograft: a randomized controlled clinical trial, *J. Periodontol.*, 2015, **86**, 348–355.

16 K. J. Burg, S. Porter and J. F. Kellam, Biomaterial developments for bone tissue engineering, *Biomaterials*, 2000, **21**, 2347–2359.

17 E. M. Ahmed, Hydrogel: Preparation, characterization, and applications: A review, *J. Adv. Res.*, 2015, **6**, 105–121.

Open Access Article. Published on 11 November 2022. Downloaded on 1/12/2026 3:45:44 PM.
This article is licensed under a Creative Commons Attribution-NonCommercial 3.0 Unported Licence.

18 R. Agarwal and A. J. Garcia, Biomaterial strategies for engineering implants for enhanced osseointegration and bone repair, *Adv. Drug Delivery Rev.*, 2015, **94**, 53–62.
19 Z. Ning, B. Tan, B. Chen, D. S. A. Lau, T. M. Wong, T. Sun, S. Peng, Z. Li and W. W. Lu, Precisely Controlled Delivery of Abaloparatide through Injectable Hydrogel to Promote Bone Regeneration, *Macromol. Biosci.*, 2019, **19**, e1900020.
20 C. Wang, K. He, J. Li and X. Chen, Conformal electrodes for on-skin digitalization, *SmartMat*, 2021, **2**, 252–262.
21 F. Antonica, D. F. Kasprzyk, A. A. Schiavo, M. Romitti and S. Costagliola, Generation of Functional Thyroid Tissue Using 3D-Based Culture of Embryonic Stem Cells, *Methods Mol. Biol.*, 2017, **1597**, 85–95.
22 S. S. Ghourichaee, E. M. Powell and J. B. Leach, Enhancement of human neural stem cell self-renewal in 3D hypoxic culture, *Biotechnol. Bioeng.*, 2017, **114**, 1096–1106.
23 M. Rafat, F. F. Li, P. Fagerholm, N. S. Lagali, M. A. Watsky, R. Munger, T. Matsuura and M. Griffith, Peg-stabilized carbodiimide crosslinked collagen-chitosan hydrogels for corneal tissue engineering, *Biomaterials*, 2008, **29**, 3960–3972.
24 N. C. Hunt, D. Hallam, A. Karimi, C. B. Mellough, J. Chen, D. H. W. Steel and M. Lako, 3D culture of human pluripotent stem cells in RGD-alginate hydrogel improves retinal tissue development, *Acta Biomater.*, 2017, **49**, 329–343.
25 S. K. Seidlits, Z. Z. Khaing, R. R. Petersen, J. D. Nickels, J. E. Vanscoy, J. B. Shear and C. E. Schmidt, The effects of hyaluronic acid hydrogels with tunable mechanical properties on neural progenitor cell differentiation, *Biomaterials*, 2010, **31**, 3930–3940.
26 Z. Liu, M. Tang, J. Zhao, R. Chai and J. Kang, Looking into the Future: Toward Advanced 3D Biomaterials for Stem-Cell-Based Regenerative Medicine, *Adv. Mater.*, 2018, **30**, e1705388.
27 M. Nagaoka, K. Si-Tayeb, T. Akaike and S. A. Duncan, Culture of human pluripotent stem cells using completely defined conditions on a recombinant E-cadherin substratum, *BMC Dev. Biol.*, 2010, **10**, 60.
28 S. M. Ibim, K. E. Uhrich, R. Bronson, S. F. El-Amin, R. S. Langer and C. T. Laurencin, Poly(anhydride-*co*-imides): *in vivo* biocompatibility in a rat model, *Biomaterials*, 1998, **19**, 941–951.
29 A. Mir, A. Kumar and U. Riaz, A short review on the synthesis and advance applications of polyaniline hydrogels, *RSC Adv.*, 2022, **12**, 19122–19132.
30 F. Liu, W. Li, H. Liu, T. Yuan, Y. Yang, W. Zhou, Y. Hu and Z. Yang, Preparation of 3D Printed Chitosan/Polyvinyl Alcohol Double Network Hydrogel Scaffolds, *Macromol. Biosci.*, 2021, **21**, e2000398.
31 C. Chen, X. W. Geng, Y. H. Pan, Y. N. Ma, Y. X. Ma, S. Z. Gao and X. J. Huang, Synthesis and characterization of tannic acid-PEG hydrogel *via* Mitsunobu polymerization, *RSC Adv.*, 2020, **10**, 1724–1732.
32 A. A. Deschamps, M. B. Claase, W. J. Sleijster, J. D. de Bruijn, D. W. Grijpma and J. Feijen, Design of segmented poly(ether ester) materials and structures for the tissue engineering of bone, *J. Controlled Release*, 2002, **78**, 175–186.
33 J. Zhu and R. E. Marchant, Design properties of hydrogel tissue-engineering scaffolds, *Expert Rev. Med. Devices*, 2011, **8**, 607–626.
34 J. Berger, M. Reist, J. M. Mayer, O. Felt, N. A. Peppas and R. Gurny, Structure and interactions in covalently and ionically crosslinked chitosan hydrogels for biomedical applications, *Eur. J. Pharm. Biopharm.*, 2004, **57**, 19–34.
35 N. R. Sudarshan, D. G. Hoover and D. Knorr, Antibacterial action of chitosan, *Food Biotechnol.*, 1992, **6**, 257–272.
36 P. Chan, M. Kurisawa, J. E. Chung and Y. Y. Yang, Synthesis and characterization of chitosan-g-poly(ethylene glycol)-folate as a non-viral carrier for tumor-targeted gene delivery, *Biomaterials*, 2007, **28**, 540–549.
37 N. Bhattarai, J. Gunn and M. Zhang, Chitosan-based hydrogels for controlled, localized drug delivery, *Adv. Drug Delivery Rev.*, 2010, **62**, 83–99.
38 Q. L. Li, Z. Q. Chen, B. W. Darvell, L. K. Liu, H. B. Jiang, Q. Zen, Q. Peng and G. M. Ou, Chitosan-phosphorylated chitosan polyelectrolyte complex hydrogel as an osteoblast carrier, *J. Biomed. Mater. Res., Part B*, 2007, **82**, 481–486.
39 A. R. Karimi, A. Khodadadi and M. Hadizadeh, A nanoporous photosensitizing hydrogel based on chitosan cross-linked by zinc phthalocyanine: an injectable and pH-stimuli responsive system for effective cancer therapy, *RSC Adv.*, 2016, **6**, 91445–91452.
40 Y. Y. Liao, Z. Fan and J. Z. Du, Photocrosslinking-Immobilized Polymer Vesicles for Lowering Temperature Triggered Drug Release, *Acta Phys.-Chim. Sin.*, 2021, **37**, 1912053.
41 C. M. Zhao, X. T. Lu, Q. Q. Hu, S. Liu and S. Guan, PVA/PEG Hybrid Hydrogels Prepared by Freeze-thawing and High Energy Electron Beam Irradiation, *Chem. Res. Chin. Univ.*, 2017, **33**, 995–999.
42 H. Yu, X. Zhang, W. Song, T. Pan, H. Wang, T. Ning, Q. Wei, H. H. K. Xu, B. Wu and D. Ma, Effects of 3-dimensional Bioprinting Alginate/Gelatin Hydrogel Scaffold Extract on Proliferation and Differentiation of Human Dental Pulp Stem Cells, *J. Endod.*, 2019, **45**, 706–715.
43 X. Xu, Z. Gu, X. Chen, C. Shi, C. Liu, M. Liu, L. Wang, M. Sun, K. Zhang, Q. Liu, Y. Shen, C. Lin, B. Yang and H. Sun, An injectable and thermosensitive hydrogel: Promoting periodontal regeneration by controlled-release of aspirin and erythropoietin, *Acta Biomater.*, 2019, **86**, 235–246.
44 T. Uehara, S. Mise-Omata, M. Matsui, Y. Tabata, R. Murali, M. Miyashin and K. Aoki, Delivery of RANKL-Binding Peptide OP3-4 Promotes BMP-2-Induced Maxillary Bone Regeneration, *J. Dent. Res.*, 2016, **95**, 665–672.
45 S. Ishikawa, D. Matsukuma, K. Iijima, M. Iijima, S. Osawa and H. Otsuka, N-Hydroxysuccinimide Bifunctionalized Triblock Cross-Linker Having Hydrolysis Property for a Biodegradable and Injectable Hydrogel System, *ACS Biomater. Sci. Eng.*, 2019, **5**, 5759–5769.
46 C. Matossian, S. Makari and R. Potvin, Cataract surgery and methods of wound closure: a review, *Clin. Ophthalmol.*, 2015, **9**, 921–928.

 © 2022 The Author(s). Published by the Royal Society of Chemistry

Open Access Article. Published on 11 November 2022. Downloaded on 1/12/2026 3:45:44 PM.
This article is licensed under a Creative Commons Attribution-NonCommercial 3.0 Unported Licence.

47 J. M. Schierholz and J. Beuth, Implant infections: a haven for opportunistic bacteria, *J. Hosp. Infect.*, 2001, **49**, 87–93.
48 K. Chindera, M. Mahato, A. K. Sharma, H. Horsley, K. Kloc-Muniak, N. F. Kamaruzzaman, S. Kumar, A. McFarlane, J. Stach, T. Bentin and L. Good, The antimicrobial polymer PHMB enters cells and selectively condenses bacterial chromosomes, *Sci. Rep.*, 2016, **6**, 23121.
49 F. Li, B. Chen, Y. Xu, F. Zhu, W. L. Ji, X. S. Wu and W. Wang, Study on the Method of Determination for PHMB and PHMG in Disinfectant, *Adm. Techn. Envir. Monit.*, 2018, **30**, 54–56.
50 N. Nallasamy, K. E. Grove, G. L. Legault, M. B. Daluvoy and T. Kim, Hydrogel ocular sealant for clear corneal incisions in cataract surgery, *J. Cataract Refractive Surg.*, 2017, **43**, 1010–1014.
51 P. Nezhad-Mokhtari, M. Ghorbani, L. Roshangar and J. S. Rad, A review on the construction of hydrogel scaffolds by various chemically techniques for tissue engineering, *Eur. Polym. J.*, 2019, **117**, 64–76.
52 H. Tanuma, T. Saito, K. Nishikawa, T. Dong, K. Yazawa and Y. Inoue, Preparation and characterization of PEG-cross-linked chitosan hydrogel films with controllable swelling and enzymatic degradation behavior, *Carbohydr. Polym.*, 2010, **80**, 260–265.
53 W. Cao, M. Cheng, Q. Ao, Y. Gong, N. Zhao and X. Zhang, Physical, mechanical and degradation properties, and schwann cell affinity of cross-linked chitosan films, *J. Biomater. Sci., Polym. Ed.*, 2005, **16**, 791–807.
54 M. C. Chang and J. Tanaka, FT-IR study for hydroxyapatite/collagen nanocomposite cross-linked by glutaraldehyde, *Biomaterials*, 2002, **23**, 4811–4818.
55 H. T. Peng, H. Huang, P. N. Shek, S. Charbonneau and M. D. Blostein, PEGylation of Melittin: Structural Characterization and Hemostatic Effects, *J. Bioact. Compat. Polym.*, 2010, **25**, 75–97.
56 F. M. Chen, M. Zhang and Z. F. Wu, Toward delivery of multiple growth factors in tissue engineering, *Biomaterials*, 2010, **31**, 6279–6308.
57 G. Rajesh Krishnan, C. Cheah and D. Sarkar, Hybrid cross-linking characteristics of hydrogel control stem cell fate, *Macromol. Biosci.*, 2015, **15**, 747–755.
58 N. Park and J. Kim, Anisotropic Hydrogels with a Multiscale Hierarchical Structure Exhibiting High Strength and Toughness for Mimicking Tendons, *ACS Appl. Mater. Interfaces*, 2022, **14**, 4479–4489.
59 G. Li, S. Li, L. Zhang, S. Chen, Z. Sun, S. Li, L. Zhang and Y. Yang, Construction of Biofunctionalized Anisotropic Hydrogel Micropatterns and Their Effect on Schwann Cell Behavior in Peripheral Nerve Regeneration, *ACS Appl. Mater. Interfaces*, 2019, **11**, 37397–37410.
60 Y. Pan, Y. Zhao, R. Kuang, H. Liu, D. Sun, T. Mao, K. Jiang, X. Yang, N. Watanabe, K. H. Mayo, Q. Lin and J. Li, Injectable hydrogel-loaded nano-hydroxyapatite that improves bone regeneration and alveolar ridge promotion, *Mater. Sci. Eng., C*, 2020, **116**, 111158.
61 H. Tan, Q. Zhou, H. Qi, D. Zhu, X. Ma and D. Xiong, Heparin interacting protein mediated assembly of nano-fibrous hydrogel scaffolds for guided stem cell differentiation, *Macromol. Biosci.*, 2012, **12**, 621–627.
62 J. A. Burdick and G. D. Prestwich, Hyaluronic acid hydrogels for biomedical applications, *Adv. Mater.*, 2011, **23**, H41–H56.
63 Y. Wen, F. Li, C. Li, Y. Yin and J. Li, High mechanical strength chitosan-based hydrogels cross-linked with poly(ethylene glycol)/polycaprolactone micelles for the controlled release of drugs/growth factors, *J. Mater. Chem. B*, 2017, **5**, 961–971.
64 B. Trappmann, J. E. Gautrot, J. T. Connelly, D. G. Strange, Y. Li, M. L. Oyen, M. A. Cohen Stuart, H. Boehm, B. Li, V. Vogel, J. P. Spatz, F. M. Watt and W. T. Huck, Extracellular-matrix tethering regulates stem-cell fate, *Nat. Mater.*, 2012, **11**, 642–649.
65 R. K. Das, V. Gocheva, R. Hammink, O. F. Zouani and A. E. Rowan, Stress-stiffening-mediated stem-cell commitment switch in soft responsive hydrogels, *Nat. Mater.*, 2016, **15**, 318–325.
66 Z. Cao, Y. Luo, Z. Li, L. Tan, X. Liu, C. Li, Y. Zheng, Z. Cui, K. W. K. Yeung, Y. Liang, S. Zhu and S. Wu, Antibacterial Hybrid Hydrogels, *Macromol. Biosci.*, 2021, **21**, e2000252.
67 F. Mohabatpour, A. Karkhaneh and A. M. Sharifi, A hydrogel/fiber composite scaffold for chondrocyte encapsulation in cartilage tissue regeneration, *RSC Adv.*, 2016, **6**, 83135–83145.